Infiltrated SrTiO3:FeCr-based anodes for metalsupported SOFC

Blennow Tullmar, Peter; Persson, Åsa Helen; Nielsen, Jimmi; Sudireddy, Bhaskar Reddy; Klemensø, Trine

Published in:
Proceedings

Publication date:
2012

Document Version
Publisher's PDF, also known as Version of record

A0908

Infiltrated $SrTiO_3$:FeCr-based anodes for metal-supported SOFC

Peter Blennow, Åsa H. Persson, Jimmi Nielsen,
Bhaskar R. Sudireddy, Trine Klemensø
Department of Energy Conversion and Storage, Technical University of Denmark,
Frederiksborgvej 399, DK-4000 Roskilde, Denmark
Tel.: +45 4677 5868
Fax: +45 4677 5858
pebl@dtu.dk

Abstract

The concept of using highly electronically conducting backbones with subsequent infiltration of electrocatalytic active materials, has recently been used to develop an alternative SOFC design based on a ferritic stainless steel support. The metal-supported SOFC is comprised of porous and highly electronically conducting layers, into which electrocatalytically active materials are infiltrated after sintering.
This paper presents the first results on single cell testing of 25 cm^2 cells with 16 cm^2 active area of a metal-supported SOFC were the anode backbone consists of a composite of Nb-doped $SrTiO_3$ (STN) and FeCr. Electrochemical characterization and post test SEM analysis have been used to get an insight into the possible degradation mechanisms of this novel electrode infiltrated with Gd-doped CeO_2 and Ni. Accelerated oxidation/corrosion experiments have been conducted to evaluate the microstructural changes occurring in the anode layer during testing. The results indicate that the STN component in the anode seems to have a positive effect on the corrosion stability of the FeCr-particles in the anode layer.

1. Introduction

Solid oxide fuel cells (SOFCs) offer the possibility of power generation with a higher efficiency than conventional combustion systems. However, in terms of cost and durability SOFCs are not yet competitive. Metal supported SOFCs (MS-SOFC) are in this context promising. Besides lower material cost with the potential use of commercial available stainless steel, MS-SOFC has some advantages compared to the traditional high (750 – 1000 ºC) and intermediate (650 – 750 ºC) temperature purely ceramic based SOFCs. These advantages are among other things higher thermal conductivity and ductility of the support, which in particular is an advantage in small-scale and mobile systems where tolerance towards e.g. the presence of shock vibrations, thermal cycling, electrical load transients, and redox cycles may be important [1-3].

The introduction of stainless steel into SOFCs raises some new challenges with respect to cell fabrication, since the usual sintering in an oxidizing atmosphere of the various components such as the electrolyte (above 1200 ºC) and the cathode (above 1000 ºC) used for conventional ceramic based SOFC fabrication needs to be avoided. The MS-SOFC design developed at DTU Energy Conversion (part of former Risø DTU) is based on a multilayered structure obtainable by cost effective ceramic processing techniques such as powder metal tape casting, lamination, co-sintering and infiltration [3,4]. The innovative concept ensures that the number of different steps in manufacturing is minimized. Based on the well known challenges with interdiffusion in the Ni-Fe-Cr system [5] and Ni coarsening during operation, an unconventional half cell design was developed [4], where these problems were circumvented by the use of an alternative anode structure. The anode layer consists of a stainless steel based cermet backbone, which as a final step in the cell fabrication is infiltrated with $Ce_{0.8}Gd_{0.2}O_{1.9}$ and minor amounts of Ni (Ni:CGO). MS-SOFCs with this type of anode have been demonstrated on single cell level (active area 16 cm^2) to show excellent performance and durability with a degradation rate of 0.9 % pr. 1000 hours during in total 3000 hours of 0.25 Acm^{-2} galvanostatic testing at 650 ºC. It was furthermore shown on button cells (active area of 0.5 cm^2) that with the combination of a dense CGO barrier layer and a LSC cathode a performance with an area specific resistance (ASR) of 0.27 Ωcm^2 at 650 ºC could be obtained [6].

Despite the very promising performance results obtained with the abovementioned metal-supported cell design, there is still a need to improve the long-term stability, especially when operating the MS-SOFC with high fuel utilization. As pointed out in [3], the developed cermet anode layer experience corrosion during cell operation, which could be detrimental for long-term stability. One way to solve these problems could be to use an anode design based on ceramic materials, such as n-doped $SrTiO_3$, e.g. Nb-doped $SrTiO_3$. Nb-doped $SrTiO_3$ has been shown to have high electronic conductivity and promising redox stability [7,8]. Recently, we reported the first results of a MS-SOFC with STN:FeCr composite in the backbone of the anode layer, into which Ni:CGO electrocatalysts were infiltrated. The button cells (active area 0.5 cm^2) showed promising initial performance, reaching power densities >1 Wcm^{-2} at 700 ºC with hydrogen as fuel [9].

This paper presents the results on single cell testing of larger cells (25 cm^2 cells with 16 cm^2 active area) of MS-SOFC with STN:FeCr-based anodes. Oxidation/corrosion experiments as well as detailed SEM analysis have been conducted to evaluate the microstructural and chemical changes occurring in the anode layer during testing. These are important aspects since the MS-SOFCs needs to be able to withstand the technological relevant condition of high fuel utilization without severe detrimental corrosion.

2. Experiments

2.1. Sample Fabrication

The cell design is based on a multilayered structure fabricated by conventional ceramic processing techniques such as tape casting and screen printing. A metal support layer (ferritic stainless steel alloy (FeCr), 22 % Cr with Fe as base) and an anode backbone layer, comprising of an electronically conducting Nb-doped $SrTiO_3$ ceramic component ($Sr_{0.99}Ti_{0.9}Nb_{0.1}O_3$, STN) and 30-50 vol.% FeCr particles, were tape casted individually and then laminated together with a tape casted electrolyte layer. The slurries prepared for tape casting were based on organic solvent and contained binder, plasticizer, and other additives (such as pore formers) needed for the fabrication of porous and/or dense layers.
The electrolyte was based on ZrO_2 co-doped with Sc_2O_3 and Y_2O_3 (from here on referred to as ScYSZ). The STN material was fabricated with solid state route with $SrCO_3$, TiO_2 and Nb_2O_5 as precursors. The precursor powders were mixed thoroughly and calcined in air at 1300 ºC for 4h, then reground and fired a second time in reducing (H_2/Ar) atmosphere at 1300 ºC for 10h. The small Sr deficiency ($Sr_{0.99}Ti_{0.9}Nb_{0.1}O_3$) was introduced to avoid any possible Sr-enriched secondary phase formation [7].
The laminated layers comprising the half cell (metal support, anode backbone layer, and electrolyte) were first heat treated in air to remove the organics in the tapes. This debinding step was followed by a co-sintering step, using a proprietary procedure, above 1100 ºC in a reducing atmosphere (H_2/Ar). After co-sintering, the electrocatalytically active phase, comprising a precursor solution of $Ce_{0.8}Gd_{0.2}O_{1.9}$ (CGO20) and Ni, was infiltrated into the porous structure of the half cell. The infiltration of electrocatalysts followed the same procedure as described elsewhere [4]. The infiltrated oxide phases amounted to approximately 3 wt% of the half cell. Next, a 1 µm thick $Ce_{0.8}Gd_{0.2}O_{1.9}$ (CGO10) interdiffusion cathode barrier layer (CBL) was deposited with PVD, as described by Klemensø et al. [6]. A cathode with composition 50 % LSC : 50 % CGO (by volume) ($(La_{0.6}Sr_{0.4})_{0.99}CoO_{3-\delta}$: $Ce_{0.9}Gd_{0.1}O_{2-\delta}$) were applied by screen printing. A LSC layer was also used as cathode contact component. A schematic of the cell design is shown in Figure 1. The layers were fired *in situ* during cell testing at maximum temperature of 800 °C as described in [6]. Note that only the half cells with 70 % STN : 30 % FeCr in the anode backbone have been used for electrochemical characterization in this work. Half cells for corrosion testing, i.e. metal support, anode backbone layer, and electrolyte, were prepared in the same way as described above. Anode backbones with 50 % STN : 50 % FeCr were included in these tests as well.

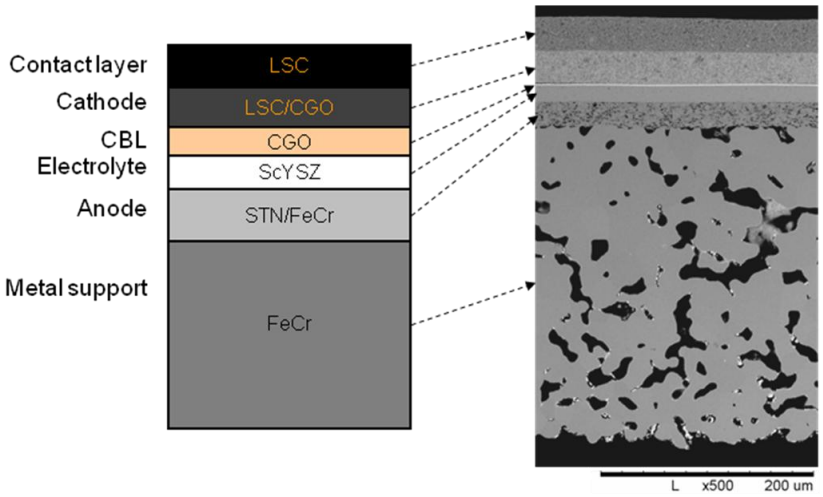

Figure 1. Schematic illustration and SEM cross-section (using backscattered electron mode) of the MS-SOFC cell with STN:FeCr (70:30) anode backbone.

2.2. Corrosion testing

Half cells infiltrated with Ni:CGO were prepared and tested for corrosion stability. The size of the samples was 10 x 10 mm. The composition of the anode backbone was varied, having either 70 % STN : 30 % FeCr or 50 % STN : 50 % FeCr. Reference half cells with the previously reported FeCr:YSZ anode backbone [6] were included for comparison. The corrosion tests were conducted in an conventional tube furnace at accelerated corrosion conditions corresponding to 850 °C in simulated outlet anode gas, i.e. an Ar-H_2-H_2O atmosphere with pH_2O/pH_2 = 9 (simulating the oxygen partial pressure at the fuel outlet when having 90 % fuel utilization). After 500 h corrosion testing the microstructure of the half cells was investigated.

2.3. Electrochemical Characterization

The footprint size of the tested cell with 70 % STN : 30 % FeCr in the anode backbone was 52x52 cm^2 and the active area 16 cm^2, which was defined by the area of the screen-printed cathode. The cell was tested in an alumina housing used for conventional anode-supported cells, and the test house and positions of voltage probes and current pick-up points were similar to as described in [10]. The Pt voltage and current probes were contacted to the current collector plates which were mounted into the test housing. A flat Ni net was used as a current collector plate on the anode side, and a Au net on the cathode side. The various gases were distributed to the cell via milled gas trenches in the alumina test housing.

Polarization curves were recorded between 650 – 750 ºC with a fuel consisting of hydrogen and 4 – 20 % water on the anode side and air or oxygen (O_2) on the cathode side. The cell was then galvanostatically durability tested for approximately 180 hours at current density of 0.25 Acm^{-2}, 650°C, with low fuel and oxygen utilisation (both below 10 %), and with H_2-3 % H_2O as fuel, and air as oxidant gas. The cell was characterised before and during SOFC operation with electrochemical impedance (EIS) measurements. Before the galvanostatic testing the cell was tested with EIS at 650 °C – 750 ºC, with H_2 fuel containing either 3 % water or 20 % water supplied to the anode, and air or oxygen supplied to the cathode. During the galvanostatic durability testing the cell was characterized simultaneously with EIS at the conditions mentioned above for the galvanostatic test. A Solartron 1255B frequency response analyser was used for the EIS measurements, which were carried out in the frequency range 0.2 Hz – 82.5 kHz.

2.4. Microstructural Characterization

The microstructure of the various samples (cells after electrochemical characterization and half cells after corrosion testing) were investigated on polished cross-sections with a Zeiss Supra 25 scanning electron microscope (SEM) equipped with an x-ray energy dispersive spectrometer (XEDS) and/or with a Hitachi TM1000 tabletop SEM operating in backscattered electron mode at 15 keV.

3. Results and Discussion

3.1. Electrochemical Characterization

Figure 2 shows polarization and power curves recorded between 650 °C and 750 °C with H_2 / 20 % H_2O as fuel and air as oxidant gas. The initial cell performance was promising, however, not as good as the previously reported values on a smaller button cell [9]. The initial ASR values were calculated as the secant value at 0.6V at the different temperatures and reached 0.43 Ωcm^2, 0.67 Ωcm^2 and 1.23 Ωcm^2 at 750 ºC, 700 ºC and 650 ºC, respectively.

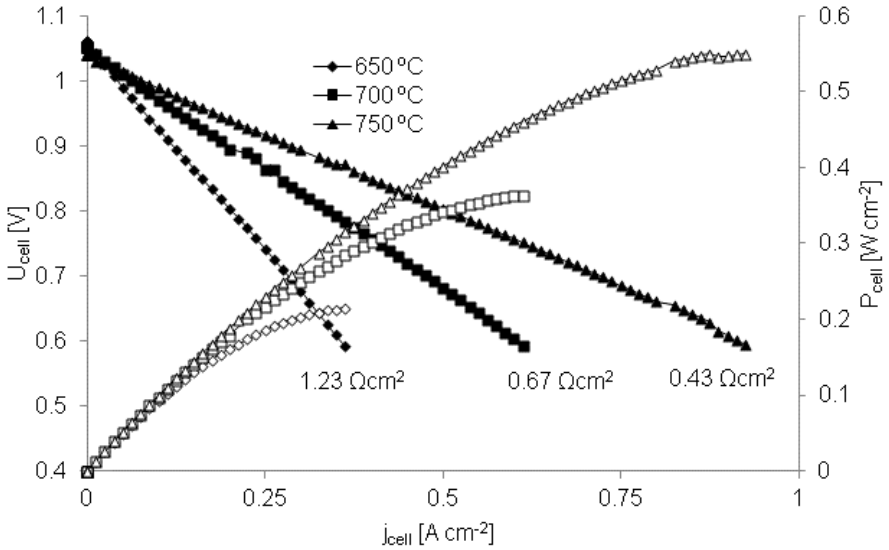

Figure 2. Polarization characteristics of the MS-SOFC at 650 – 750 ºC. H_2 with 20 % H_2O as fuel and air as oxidant. The inserted numbers are initial ASR values at the respective temperatures.

Figure 3 shows the EIS data of the cell tested at 650 ºC with H_2 / 20 % H_2O as fuel and different oxidant gases to the cathode side (air or oxygen, respectively). There was virtually no difference in the two impedance spectra, only a very small decrease in polarization resistance when changing the gases from air to pure oxygen.

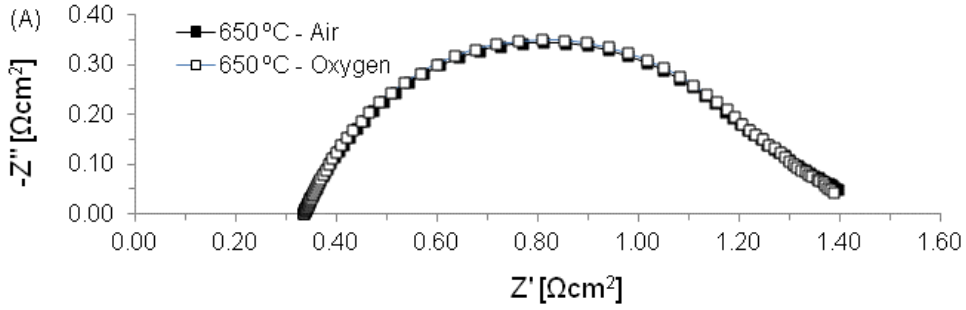

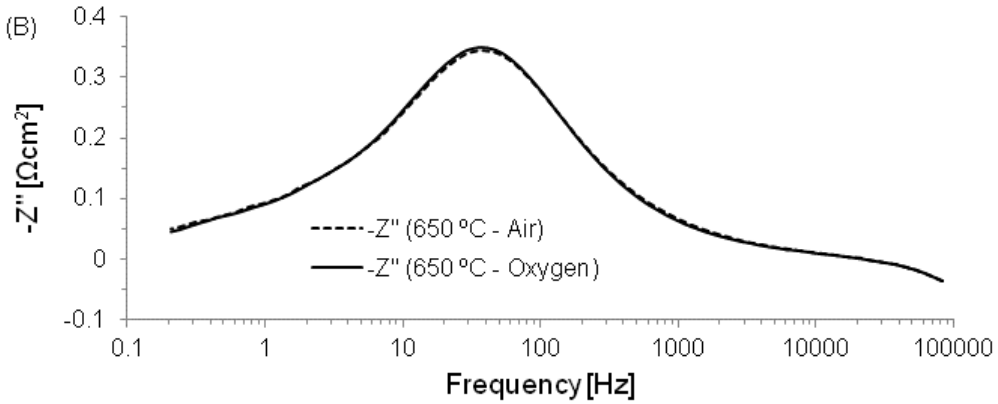

Figure 3. (A) Nyquist representation of EIS data at 650 ºC with different oxygen content to the cathode (air or pure oxygen) and H_2-20 %H_2O as fuel. (B) Bode representation of –Z'' from the test in (A).

These results indicate that the LSC:CGO-based cathode has a very low contribution to the overall polarization resistance (R_P) of the cell. Since the performance of the cathode is sensitive to the pO_2 a larger difference would be expected if the cathode had a significant contribution to the overall polarization resistance. It was recently shown that a similar LSC-based cathode with a dense CGO barrier layer on a MS-SOFC design with a FeCr:YSZ-based anode backbone (using similar Ni:CGO infiltration as in this work) had an ASR of 0.56 Ωcm^2 [6]. Therefore, the Ni:CGO-infiltrated STN:FeCr (70:30) anode backbone is thus believed to be the main reason for the relatively high ASR values obtained in the present study.

Another contributing factor is the series resistance, R_S, which is normally ascribed to the resistance from the electrolyte. However, it also contains the contribution from resistive components in the cell such as contact (constriction) resistances and/or poorly conducting layers. For a completely dense ScYSZ electrolyte with 16 µm thickness, which was the electrolyte thickness of the MS-SOFC used in this work, the electrolyte's contribution to R_S should be slightly less than 0.1 Ωcm^2 at 650 ºC [11]. Since the R_S measured in Figure 3 is more than three times larger than this value indicates that (i) the electrolyte quality is not perfect and/or (ii) there is additional contact/constriction resistance possibly due to insufficient electronic conductivity of the STN component in the backbone layer. Unfortunately, there is presently too little data available to correctly determine the reasons for the high R_S and/or high polarization resistance of the anode. Studies are currently ongoing and these results will be published in future journal papers. It is unfortunately outside the scope of this paper to discuss the electrode mechanisms of the anode and other loss mechanisms in detail.

Following the initial characterization of the cell a relatively short galvanostatic durability test was conducted. The cell was tested for approximately 180 h at 650 ºC and 0.25 Acm^{-2} where the fuel and oxygen utilization were both below 10 %. During the durability test the cell showed some initial instability, however, after 20 h the cell voltage reached a steady value around 740 mV (see Figure 4). The cell voltage remained constant during the testing period. Since this was a relatively short durability test under mild conditions (low fuel utilization) more extended durability tests are currently being conducted in order to properly evaluate the long term stability of this MS-SOFC design.

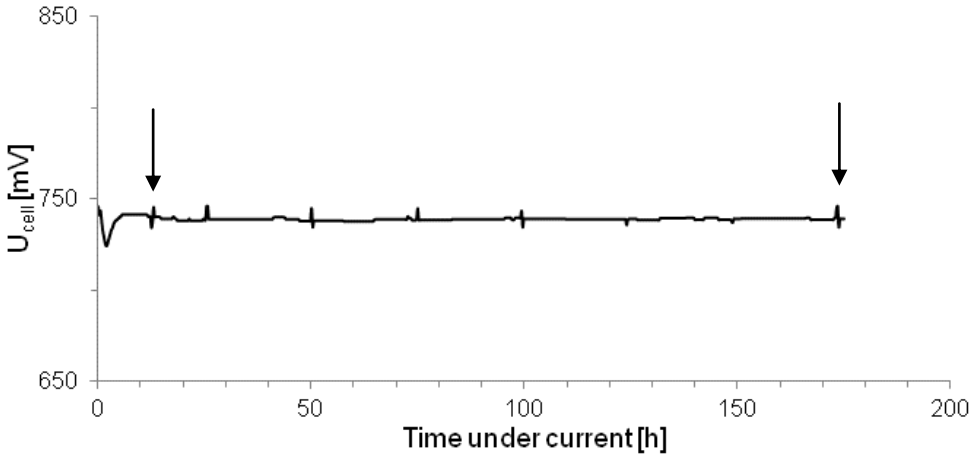

Figure 4. Galvanostatic durability curve recorded at 650 ºC, with a current density of 0.25 Acm^{-2} and humidified hydrogen (approximately 4 % H_2O) as fuel and air as oxidant. The fuel and oxygen utilization were both < 10 %. The arrows indicate when EIS were conducted under current load, as presented in Figure 5.

The spikes that are seen in the durability curve in Figure 4 are when an impedance spectra was recorded simultaneously under current load. Two selected EIS are shown in Figure 5, after 13 h testing and 174 h testing (as indicated by the arrows in Figure 4).

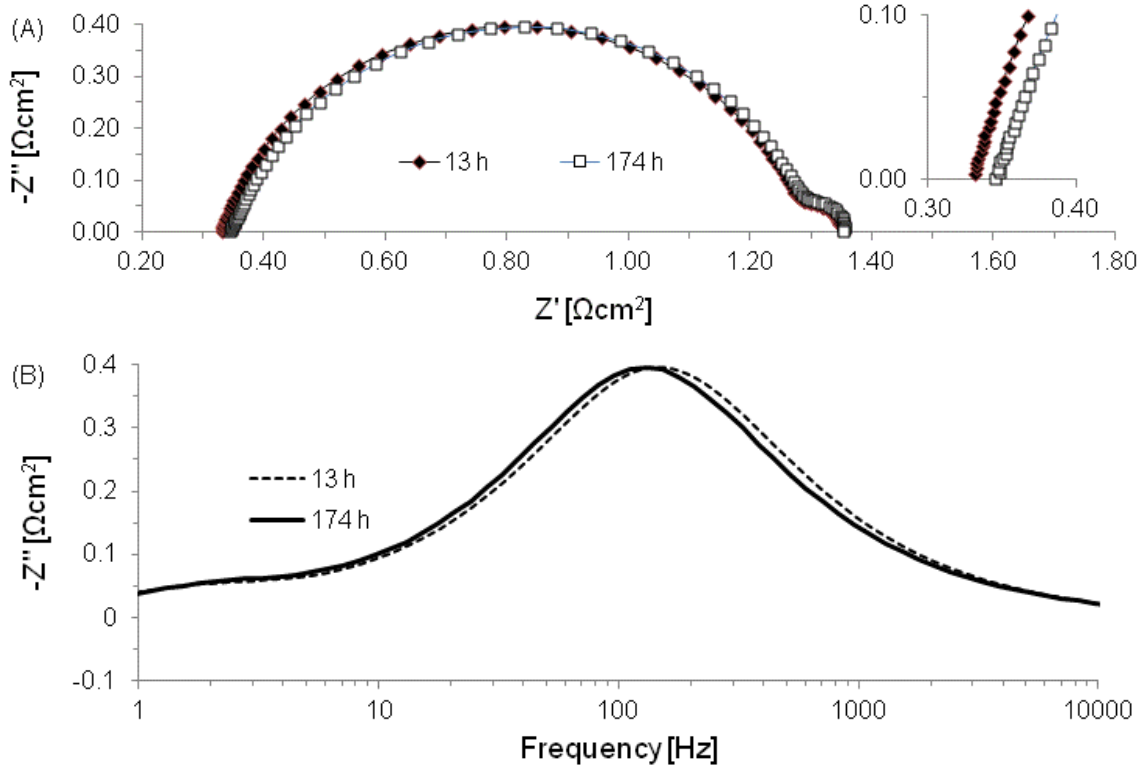

Figure 5. (A) Nyquist representation of EIS data for the cell during galvanostatic durability testing (see Figure 4). The time corresponds to the arrows indicated in Figure 4. The EIS were recorded at 650 °C with H_2-4 %H_2O as fuel and air as oxidant at a current density of 0.25 Acm^{-2}. The inset is a magnified area of the high frequency part of the impedance spectra. (B) Bode representation of –Z'' from the test in (A). Only the frequency interval where minor changes occurred is shown.

The Bode representation in Figure 5B in combination with Figure 5A illustrates the minor change in impedance behaviour of the cell during the galvanostatic durability test. The serial resistance of the cell increased slightly; however, this was compensated by a similar small decrease in the polarization resistance resulting in an identical ASR at the start and at the end of the durability test.

In order to understand the slight increase in R_S during the durability testing one has to consider the electronic conductivity properties of the STN phase. The half cells were sintered in reducing conditions (H_2/Ar) at temperatures >1100 ºC. The thermal history, and its effect on conductivity, is very important for these types of n-doped $SrTiO_3$ [12-15]. The conductivity of Nb-doped $SrTiO_3$ is dependent on the pO_2 (and temperature) [7,16]. Since the pO_2 and temperature at the testing conditions differ significantly from the conditions during sintering of the half cell, the conductivity of the titanate will subsequently be affected. The time needed to reach “conductivity equilibrium” is usually extremely long. The reason is due to the extremely slow diffusion kinetics of strontium ions and strontium vacancies and/or the very slow kinetics for incorporating oxygen in these titanates [17-19].

In order to decrease the conductivity dependence of the STN phase the FeCr : STN ratio in the anode backbone was increased in some of the half cells. These cells have not yet been characterized electrochemically, only the corrosion behavior has been investigated (see section 3.2). Increasing the FeCr : STN ratio will make the FeCr phase electronically percolating (as is the case in our previously reported FeCr:YSZ anode backbones [3,4,6]) and limit the conductivity dependence of the STN phase. Having only 30 % FeCr in the anode results in isolated FeCr particles and the STN phase will be the electronically percolated phase. However, increasing the FeCr content in the backbone layer should only be done if the potential corrosion of the metal particles can be significantly reduced.

3.2. Microstructural Characterization

SEM micrographs of cross-sections of the anode backbone layer, closest to the electrolyte, of various MS-SOFC cell designs after electrochemical testing are shown in Figure 6. A tested cell with FeCr:YSZ-based backbone has been included for comparison to show the microstructural effect of the STN phase on the corrosion of the FeCr particles.

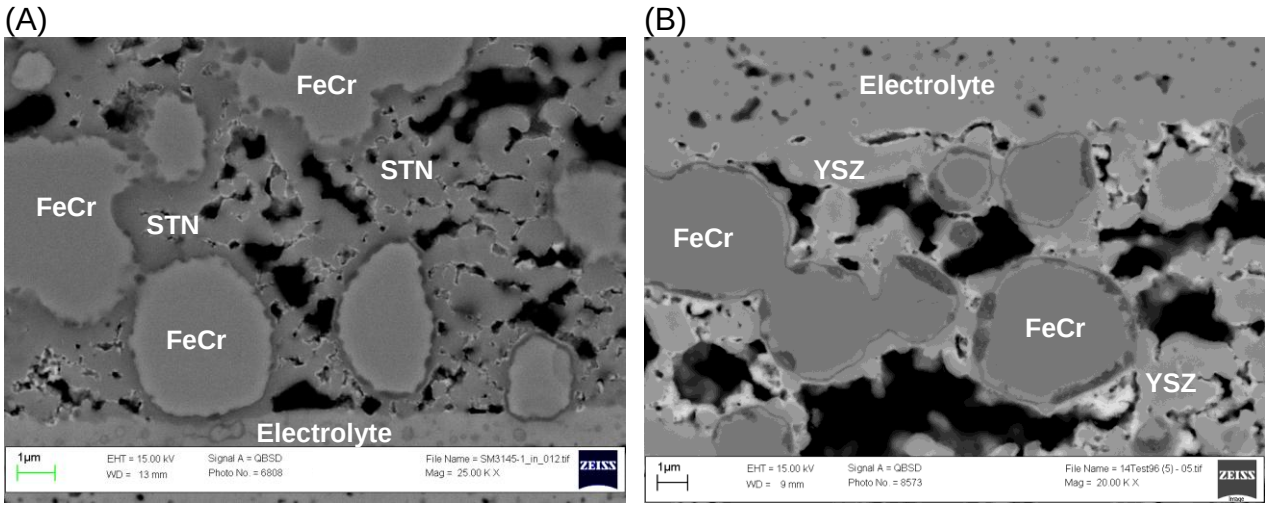

Figure 6. SEM images showing polished cross-sections of the two types of planar metal-supported half cells after electrochemical testing. (A) The tested cell having 70 % STN : 30 % FeCr in the anode backbone. (B) A tested cell having 60 % FeCr : 40 % YSZ in the anode backbone. The cells had been tested with a similar test protocol. The thin bright phase covering the backbone particles in both images is the infiltrated Ni:CGO.

Figure 6B clearly shows that there is a Cr_2O_3 scale formed on the FeCr particles in the FeCr : YSZ based anode (seen as the dark rim/areas surrounding the FeCr particles). The formation of Cr_2O_3 is expected on these stainless steels, however, the continuous growth has to be limited in order to avoid so called breakaway oxidation of the metal particles [20] and to maintain a high electronic conductivity and performance of the anode layer [3].
The formation of Cr_2O_3 on the FeCr particles in the STN : FeCr based anode seemed to be slightly different (see Figure 6A). Only a few FeCr particles showed a clear Cr-enrichment on the surface (verified by EDS but not presented here). At this point the mechanism behind the interaction of STN and FeCr is not completely clear. The chemical compatibility between STN and the other half cell components was investigated in a previous publication [9] where no indications of any formation of secondary phases were seen. STN in reducing environment is almost a pure electronically conducting ceramic [7] with no or very low oxygen ion conductivity. Since the STN seems to cover most of the FeCr particles in the anode backbone (see Figure 6A) it implies that the oxygen access to FeCr surface is limited. This will in turn have a positive effect on the corrosion resistance of the anode layer and thereby reduce the formation of Cr_2O_3.

The microstructure of the various MS-SOFC half cell designs (with Ni:CGO infiltration) corrosion tested for 500h at 850 ºC in simulated out let gas (see section 2.2) were investigated and the results are shown in Figure 7. The as-sintered half cells before test are included as well for comparison. The micrographs in Figure 7 clearly show the detrimental effect on the cell integrity of the corrosion of the FeCr particles in the anode backbone layer. There is an obvious beneficial effect of introducing the STN in the anode layer, compared with having YSZ, which is an oxygen ion conductor. After 500 h of accelerated corrosion testing at 850 ºC the FeCr particles in the FeCr : YSZ based anode have completely oxidized, which resulted in detrimental mechanical failure of the anode layer and electrolyte. Even though the FeCr particles in the STN : FeCr based anodes also have experienced severe oxidation the corrosion is not as detrimental. The half cell with 50 % STN : 50 % FeCr based anode showed the lowest oxidation. Analysis is still ongoing in order to understand this corrosion behaviour in more detail. One tentative explanation for the improved oxidation resistance of the STN : FeCr (50:50) based anode is that the microstructure of the anode backbone was improved compared with the STN : FeCr (70:30). The FeCr particles were physically better connected to the metal support, meaning that there will be a larger Cr-reservoir present which can assist in the formation of Cr_2O_3 before the FeCr particles reach a critical low Cr-content and breakaway oxidation occur [20]. Furthermore, the STN phase seemed to cover the FeCr particles better and thereby potentially isolating them in a better way from the surrounding atmosphere. The combination of Nb-doped $SrTiO_3$ with metal supported SOFC based on ferritic stainless steel therefore seems to be a promising alternative to reduce the corrosion or Cr_2O_3 formation on the FeCr particles in the anode backbone layer. By improving the microstructure and optimizing the ratio between FeCr and STN in the anode layer it is believed that the performance and durability of these types of metal supported cells will be further improved.

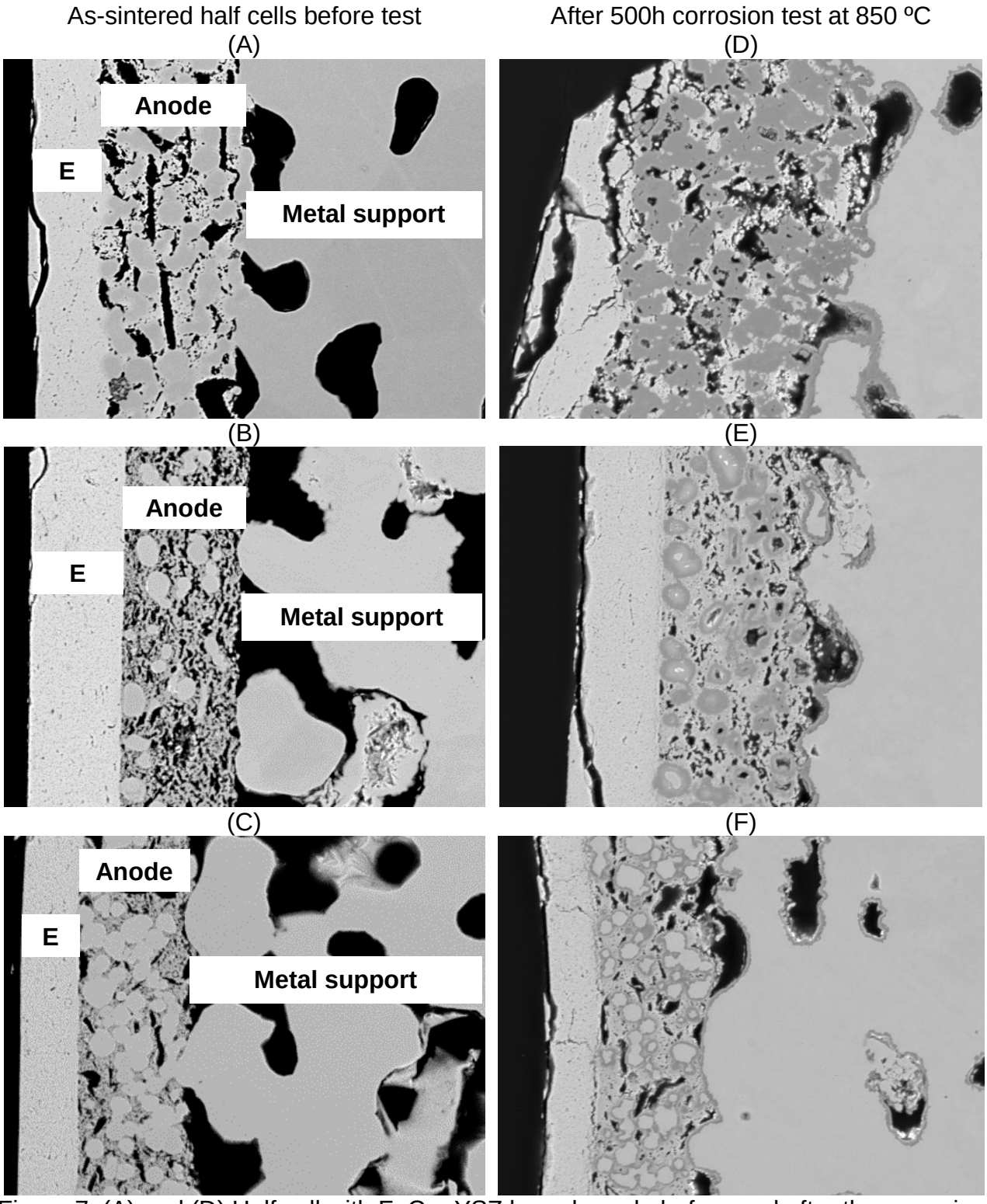

Figure 7. (A) and (D) Half cell with FeCr : YSZ based anode before and after the corrosion test. (B) and (E) Half cell with FeCr : STN (30:70) based anode before and after the corrosion test. (C) and (F) Half cell with FeCr : STN (50:50) based anode before and after the corrosion test. The “E” in the images corresponds to the electrolyte layer.

4. Conclusion

The performance and corrosion stability results presented in this work illustrate the possibility to implement a $SrTiO_3$-based anode with metal-supported cells. Combining the prospects of further improved properties of these materials with the potential robustness of the metal-supported cell design could be beneficial from a performance and long-term stability point of view. Limiting the access of oxygen (ions) to the stainless steel surface in the anode backbone, by only having electronically conducting phases, seems to be the a promising route for continuous research and development. Additional work is required to optimize the microstructure and to investigate the long term stability of the STN-based anode in the metal-supported SOFC design.

Acknowledgement

Financial support by Topsoe Fuel Cell A/S, the EU projects FP7-211940 (METSOFC) and FP7-278257 (METSAPP), The Danish National Advanced Technology Foundation, and Energinet.dk under the project ForskEL 2012-1-10806 is gratefully acknowledged.

References

[1] M.C. Tucker, G.Y. Lau, C.P. Jacobson, L.C. DeJonghe, S.J. Visco, Performance of metal-supported SOFCs with infiltrated electrodes, J. Power Sources, 171 (2007) 477-482.

[2] M.C. Tucker, Progress in metal-supported solid oxide fuel cells: A review, J. Power Sources, 195 (2010) 4570-4582.

[3] P. Blennow, J. Hjelm, T. Klemensø, S. Ramousse, A. Kromp, A. Leonide, A. Weber, Manufacturing and characterization of metal-supported solid oxide fuel cells, J. Power Sources, 196 (2011) 7117-7125.

[4] P. Blennow, J. Hjelm, T. Klemensø, Å.H. Persson, S. Ramousse, M. Mogensen, Planar Metal-Supported SOFC with Novel Cermet Anode, Fuel Cells, 11 (2011) 661-668.

[5] M. Brandner, M. Bram, J. Froitzheim, H.P. Buchkremer, D. Stoever, Electrically conductive diffusion barrier layers for metal-supported SOFC, Solid State Ionics, 179 (2008) 1501-1504.

[6] T. Klemensø, J. Nielsen, P. Blennow, Å.H. Persson, T. Stegk, B.H. Christensen, S. Sonderby, High performance metal-supported solid oxide fuel cells with Gd-doped ceria barrier layers, J. Power Sources, 196 (2011) 9459-9466.

[7] P. Blennow, A. Hagen, K.K. Hansen, L.R. Wallenberg, M. Mogensen, Defect and electrical transport properties of Nb-doped $SrTiO_3$, Solid State Ionics, 179 (2008) 2047-2058.

[8] P. Blennow, K.K. Hansen, L.R. Wallenberg, M. Mogensen, Electrochemical characterization and redox behavior of Nb-doped $SrTiO_3$, Solid State Ionics, 180 (2009) 63-70.

[9] P. Blennow, T. Klemensø, Å. Persson, K. Brodersen, A.K. Srivastava, B.R. Sudireddy, S. Ramousse, M. Mogensen, Metal-Supported SOFC with Ceramic-Based Anode, ECS Trans., 35 (2011) 683-692.

[10] S.C. Singhal, K. Kendall, Chapter 10: Testing of Electrodes, Cells and Short Stacks, , High Temperature Solid Oxide Fuel Cells: Fundamentals, Design and Applications, Elsevier Advanced Technology, Oxford, UK, 2003, pp. 261-292.

[11] S. Omar, W. Bin Najib, W. Chen, N. Bonanos, Electrical Conductivity of 10 mol% Sc_2O_3-1 mol% M_2O_3-ZrO_2 Ceramics, J. Am. Ceram. Soc., (2012), doi: 10.1111/j.1551-2916.2012.05126.x.

[12] O.A. Marina, N.L. Canfield, J.W. Stevenson, Thermal, electrical, and electrocatalytical properties of lanthanum-doped strontium titanate, Solid State Ionics, 149 (2002) 21-28.

[13] S.Q. Hui, A. Petric, Electrical properties of yttrium-doped strontium titanate under reducing conditions, J. Electrochem. Soc., 149 (2002) J1-J10.

[14] T. Kolodiazhnyi, A. Petric, The Applicability of Sr-deficient n-type $SrTiO_3$ for SOFC Anodes, J. Electroceram., 15 (2005) 5-11.

[15] P.R. Slater, D.P. Fagg, J.T.S. Irvine, Synthesis and electrical characterisation of doped perovskite titanates as potential anode materials for solid oxide fuel cells, J. Mater. Chem., 7 (1997) 2495-2498.

[16] J.T.S. Irvine, P.R. Slater, P.A. Wright, Synthesis and electrical characterisation of the perovskite niobate-titanates, $Sr_{(1-x/2)}Ti_{(1-x)}Nb_{(x)}O_{(3-d)}$, Ionics, 2 (1996) 213-216.

[17] U. Kiessling, J. Claus, G. Borchardt, S. Weber, S. Scherrer, Oxygen Tracer Diffusion in Lanthanum-Doped Single-Crystal Strontium-Titanate, J. Am. Ceram. Soc., 77 (1994) 2188-2190.

[18] R. Meyer, R. Waser, J. Helmbold, G. Borchardt, Observation of Vacancy Defect Migration in the Cation Sublattice of Complex Oxides by O18 Tracer Experiments, Phys. Rev. Lett., 90 (2003) 105901.

[19] K. Gomann, G. Bochardt, M. Schulz, A. Gomann, W. Maus-Friedrichs, B. Lesage, O. Kaitasov, S. Hoffman-Eifert, T. Schneller, Sr diffusion in undoped and La-doped $SrTiO_3$ single crystals under oxidizing conditions, Phys. Chem. Chem. Phys., 7 (2005) 2053-2060.

[20] H.E. Evans, A.T. Donaldson, T.C. Gilmour, Mechanisms of breakaway oxidation and application to a chromia-forming steel, Oxid. Met., 52 (1999) 379-402.